RSC Advances

ROYAL SOCIETY OF CHEMISTRY

www.rsc.org/advances

ARTICLE

Ceramide increases free volume voids in DPPC membranes

E. Axpe[a,CO], A. B. García-Arribas[b,c,CO], J. I. Mujika[d,CO], D. Mérida[a], A. Alonso[b,c], X. Lopez[d], J. A. García[e], J. M. Ugalde[d], F. M. Goñi[b,c] and F. Plazaola[a].

Cite this: DOI: 10.1039/x0xx00000x

Received 00th January 2014,
Accepted 00th March 2014

DOI: 10.1039/x0xx00000x

www.rsc.org/

Positron annihilation lifetime spectroscopy (PALS) can measure changes in local free volume voids in lipid bilayers. PALS has been applied, together with differential scanning calorimetry (DSC) and molecular dynamics (MD) simulations, to study free volume voids in DPPC and DPPC:ceramide (85:15 mol:mol) model membranes in the 20-60 ºC range. The free volume void average size clearly increases with the gel-fluid phase transition of the lipid, or lipid mixture. Ceramide increases void size at all temperatures, particularly in the range causing the gel-fluid transition of the mixture. A parallel study of PALS and calorimetric data indicates that, for the complex thermotropic transition of the DPPC:ceramide mixture, PALS is detecting the transition of the DPPC component, while calorimetry changes indicate mainly the melting of the ceramide-enriched domains. Molecular dynamics calculations provide a clear distinction between ceramide-rich and -poor domains, and show that the voids are predominantly located near the membrane nodal plane. The ceramide-induced increase in void volume size occurs as well at temperatures when both phospholipid and ceramide are in the fluid state, indicating that the effect is not the result of phospholipid-ceramide domain coexistence. The above observations may be related to hitherto unexplained properties of ceramide, such as the increase in membrane permeability, and the induction of transmembrane (flip-flop) lipid motion.

Introduction

Ceramides (Cer), a family of bioactive sphingolipids, are a key factor in cellular signaling.[1-5] A variety of cellular processes, from cell proliferation to apoptosis (programmed cell death), are mediated by Cer.[6] Long-chain Cer, due to their high hydrophobicity, have been proposed to exert their cell death-inducing effect through alterations of membrane biophysical properties.[7-9] In particular, long-chain Cer (palmitoylceramide) affects the properties of model lipid membranes: e.g., increases solute efflux by permeation across the membrane,[10, 11] alters the diffusion of lipids between the inner and outer leaflets of lipid bilayers ("flip-flop")[12] and generates micron-sized Cer-enriched domains with a high degree of intermolecular packing.[13-17] These Cer-enriched domains have been described as well in induced hot-cold hemolysis of erythrocytes[18] and in the mitochondrial outer membrane of mammalian cells upon irradiation stress and are essential for apoptosis through the intrinsic pathway.[19]

Nanometric free volume voids are crucial for several structural and dynamic properties of biomembranes: e.g., packing and ordering of molecules of the bilayer,[20] diffusion of lipids and proteins in its plane[21-23] and permeation of small molecules across the membrane.[24] However, the particular effect of Cer on free volume voids inside membranes remains unknown. The difficulties in the analysis of nanometer- and subnanometer-sized voids in biomembranes via non-perturbative experiments might be the cause of this lack of knowledge. Furthermore, free volume voids could be involved in the hitherto unknown mechanism of certain Cer properties, e.g. lateral separation of domains, membrane permeabilization, or transbilayer lipid movements (flip-flop).

We hypothesized that the presence of Cer affects free volume void size and distribution in membranes. To prove this statement, we used positron annihilation lifetime spectroscopy (PALS) to characterize the free volume voids in DPPC model lipid membranes with/without egg Cer, which contains ~ 85% N-palmitoylceramide. DPPC is a phospholipid widely used and studied in the membrane biophysics field despite occurring in nature as a pulmonary surfactant and not as an actual membrane component. However, properties of DPPC molecules and DPPC membrane structures as model lipid systems have been well-described through a wide variety of techniques. PALS is the only technique to gauge changes of local free volume voids in biomolecular systems.[25, 26] We demonstrate that PALS measurements, complemented by DSC and atomistic molecular dynamics simulations, are able to characterize free volume changes caused by ceramides in the voids inside model membranes. The experimental results obtained in this work open the door for the study of free volume changes when different proteins or other molecules are present in cell membranes.

Experimental

Chemicals

Egg-yolk ceramide (Cer), 1,2-dipalmitoyl-*sn*-glycero-3-phosphocholine (DPPC) and 1,2-dioleoyl-*sn*-glycero-3-phosphocholine (DOPC) were purchased from Avanti Polar Lipids (Alabaster, AL, USA).

Membrane preparation

Multilamellar vesicles (MLVs) were prepared by initially mixing the appropriate amount of synthetic pure lipids dissolved in chloroform/methanol (2:1, v/v). The samples were dried by

evaporating the solvent under a stream of nitrogen, then placing them under high vacuum for 2 h. The samples were then hydrated in purified water (lipid:water 40:60 w/w for PALS, 1 mM lipid in buffer for DSC), helping dispersion by stirring with a glass rod and finally extruding the solutions between two syringes through a narrow tubing (0.5 mm internal diameter, 10 cm long) 150 times. The procedure was performed at a temperature well above that of the phase transitions for all compositions.

Differential Scanning Calorimetry

The measurements were performed in a VP-DSC high-sensitivity scanning microcalorimeter (MicroCal, Northampton, MA, USA). Both lipid and buffer solutions were fully degassed prior to loading into the appropriate cell in the form of MLVs. MLVs were prepared as described previously, but in assay buffer (NaCl 150 mM, 20 mM PIPES, 1 mM EDTA) and at a 1 mM concentration. A final amount of 0.5 ml at 1 mM total lipid concentration was loaded into the calorimeter, performing three heating scans at a 45 ºC/h rate, between 20 and 70 ºC for all samples. Phospholipid concentration was determined as lipid phosphorus, and used together with data from the third scan, to obtain normalized thermograms. The software Origin 7.0 (MicroCal), provided with the calorimeter, was used to determine the different thermodynamic parameters from the scans. The software PeakFit (Systat Software Inc., Chicago, IL, USA) was used for endotherm deconvolution.

Positron annihilation lifetime spectroscopy (PALS)

PALS measurements were performed using an ORTEC (Oak Ridge, TN, USA) fast-fast coincidence system, two BC-422 Saint Gobain (Hiram, OH, USA) plastic scintillators and two H1949-50 photo multipliers made by Hamamatsu Photonics (Tokyo, Japan) placed in a vertical position inside of a FFD-1402 refrigerator from Radiber S.A. (Barcelona, Spain). The resolution function was 260 ps. The temperature of the samples was controlled by an Eurotherm (United Kingdom) 3508 programmable temperature control system equipped with a variable power supply provided by SALICRU (Bilbao, Spain), a 100W FIREROD® cartridge heater from Watlow Europe (Kronau, Germany), and a PT-100 CS5 (1|5) temperature sensor purchased from TC S.A. (Madrid, Spain). This PT-100 and the heater were installed in an aluminium sample holder. The manufacturing of the ^{22}NaCl sealed source of 15 μCi was described in detail in a previous article[27]. The positron source was sandwiched between two identical samples.

Around $3{\cdot}10^6$ counts per spectrum were collected for each positron lifetime spectrum. LT_polymers program[28] was used for the lifetime analysis. The source contribution (31.55%, 0.382 ns) was subtracted and three lifetime components were obtained. The longest-lived lifetimes presented distributions, and the average values of these distributions were used as ortho-positronium (o-Ps) components for analysis and free volume void size calculations. As in previous PALS studies in lipid membranes [26], Tao-Eldrup model equation was employed to estimate the average free volume hole radius:[29, 30]

$$\tau_{o-Ps}^{-1}[\mathrm{ns}] = 2(\mathrm{ns})^{-1}\left[1 - \frac{R}{R_0} + \frac{1}{2\pi}\sin\left(\frac{2\pi R}{R_0}\right)\right]$$

where $R_0 = R + \Delta R$, ΔR being an empirical parameter fitted to 1.66 Å[31]. The average free volume void size was evaluated, assuming spherical voids as

$$V_f = \frac{4}{3}\pi R^3$$

Molecular dynamics simulations

Two model bilayers were studied by atomistic molecular dynamics simulations: DPPC in solution and DPPC+C16:0 type ceramide in solution. Each system was simulated at four temperatures: 20 ºC, 30 ºC, 37 ºC and 52 ºC. The initial structure and topology files for the DPPC in solution system were taken from the web page of the Biocomputing group at the University of Calgary[32]. The structure is composed of 128 DPPC lipids, 64 per leaflet. For the DPPC+Cer system, 24 DPPC molecules were replaced by ceramide molecules, giving rise to a mixture of 18% Cer in DPPC. The force field parameters for Cer were adjusted from the topology file downloaded from R. Faller's web page.[33]

The Gromacs package (version 4.5.3)[34, 35] was employed to run all molecular dynamics simulations. The united atom GROMOS lipid force field, including the parametrization scheme proposed by Berger was employed for the lipids.[36] Periodic boundary conditions were considered by defining an orthorhombic cell. The system was solvated by adding a total of 5726 SPC model water molecules.

All simulations were carried out under isothermal–isobaric ensemble (NPT) conditions using Nose-Hoover temperature (at 20 ºC, 30 ºC, 37 ºC or 52 ºC)[37] and Parrinello-Rahman pressure coupling (1 atm).[38] The temperature of the lipids and the solvent were independently coupled. Long-range electrostatics were calculated using the smooth particle mesh Ewald (PME) method,[39] with a fourth-order spline and 0.12 nm grid spacing. A cut-off of 10 Å was defined for the electrostatics and van der Waals non-bonded interaction and neighbor-list. All bond lengths were constrained by means of Linear Constraint Solver (LINCS),[40] allowing an integration time step of 2 fs. A total run of 100 ns simulation time was carried out for the production stage of each simulation. Note that due to limitations in computational capacity, the number of molecules is not enough to represent macro, or even microscale, phase separation.

Free volume determination

A grid-based method was employed to determine the free volume in each bilayer model. The protocol is based on a previous work:[26] a rectangular 3D grid is defined for a particular structure, and the number of free grid spots counted. A given grid spot is considered occupied when at least one of the atoms constituting the system is within its van der Waals radius. Sane et al. employed a grid element length of 0.75 Å. In addition, they characterized the "accessible free volume" by including a fictitious spherical particle. Since a diameter of 1.59 Å was calculated theoretically for a positronium,[41] we increased the grid element length to 1.6 Å and did not employ any fictitious spherical particle.

The results provided by PALS experiments are directly related to the average size of the voids located in the system. Analogously, the average voids' size was evaluated from the molecular dynamics simulations. To do so, first the sizes of all voids present in a given structure extracted from a MD simulation were determined by a union/find algorithm, i. e. all grid elements in close contact belong to the same void particle. Once the voids of different sizes were determined, the average void size in a given structure was determined.

Membrane models are fluctuating dynamic systems and therefore the free volume may differ substantially from two different snapshots of the same simulation. Thus, a correct sampling of the system is crucial in order to calculate properly a meaningful average. Since the free volume characterized by the grid-based method is carried out on individual structures, 10 snapshots were extracted from the last 10 ns of each simulation (one every 1ns), and the average void size and standard deviation determined for each MD simulation. These 10 structures were also employed to calculate a number of additional properties, including lipid CD order parameter.

Results and discussion

To test whether free volume void sizes of lipid membranes are affected by Cer, we compared the mean void sizes for pure DPPC and DPPC:Cer (85:15 mol:mol) at various temperatures (Fig. 1).

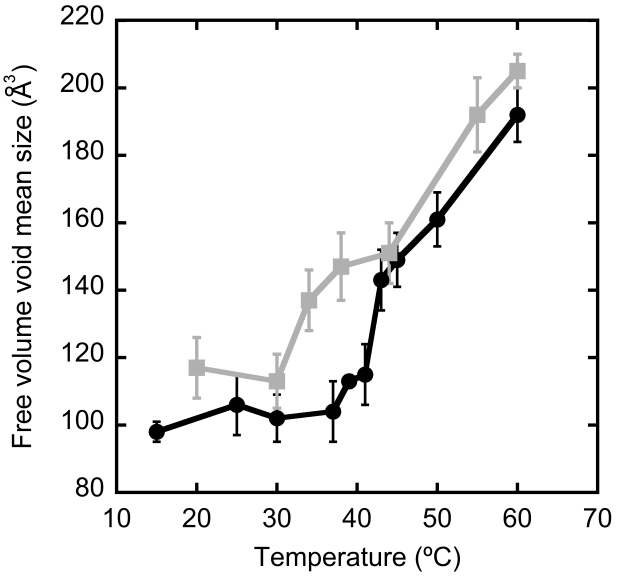

Fig. 1 Temperature dependence of free volume void mean size in DPPC membranes (black) and in DPPC:Cer (85:15 mol:mol) (grey).

Table 1 shows ortho-positronium (o-Ps) mean lifetimes and distributions in the two investigated membrane systems, as obtained by PALS. Fig. 1 shows that the average void size in pure DPPC bilayers increases with temperature. Void size remains more or less constant up to 37 ºC, and increases steeply afterwards. The highest slope is recorded between 41 ºC and 43 ºC, i.e. at the gel-fluid transition temperature of DPPC.[42] When DPPC:Cer bilayers are examined (Fig. 1) Cer is seen to enhance the mean free volume void size for most temperatures. The most striking difference corresponds to the DPPC transition temperature range. At 37 ºC the mean void size was 104±2 Å^3 for DPPC, while for DPPC:Cer the void size at 38 ºC was ~ 40% larger, 147±2 Å^3. The o-Ps lifetime distribution is wider in the presence of Cer (see Table 1). This means that the size difference between the free volume holes is larger for the Cer-containing bilayer.

Differential scanning calorimetry (DSC) experiments (Fig. 2) show the thermotropic behavior of lipid membranes. Lipid gel-fluid phase transitions can be easily identified as endotherms (Fig. 2A). DOPC did not render any endothermic peak in the temperature range under study as its gel-fluid transition is far below 10 ºC. DPPC exhibits a main endotherm at ~ 41 ºC, corresponding to the gel-fluid (or liquid-crystalline) phase transition, and a smaller one at ~ 35 ºC, the so-called pretransition, occurring between a tilted and a rippled gel phase. The DPPC:Cer binary mixture shows a very wide and complex transition, from a gel phase at 20 – 25 ºC to a fluid state at 55 – 60 ºC. The endotherm can be decomposed in at least three partially overlapping signals, corresponding probably to coexisting DPPC:Cer domains of non-uniform composition. Pure ceramide undergoes a solid-fluid transition at a narrow temperature interval, above 90 ºC.

The effects of Cer on the thermotropic properties of lipid transitions have been described.[9, 16] The DPPC:Cer thermogram is in accordance with previously published data for other lipid ratios of this[17] and related lipid mixtures.[43, 44] In general, long-chain ceramides have the effect of increasing the temperature and of widening the phospholipid gel-liquid phase transitions.

DPPC

T (ºC)	$<\tau_{o-Ps}>$ (ns)	σ_{o-Ps} (ns)
15	2.02 ± 0.03	0.35 ± 0.03
25	2.10 ± 0.09	0.34 ± 0.11
30	2.05 ± 0.07	0.47 ± 0.09
37	2.07 ± 0.09	0.60 ± 0.10
39	2.17 ± 0.01	0.61 ± 0.02
41	2.19 ± 0.09	0.63 ± 0.10
43	2.47 ± 0.09	0.73 ± 0.10
45	2.53 ± 0.07	0.71 ± 0.10
50	2.65 ± 0.07	0.69 ± 0.10
60	2.93 ± 0.07	0.46 ± 0.15

DPPC:Cer (85:15)

T (ºC)	$<\tau_{o-Ps}>$ (ns)	σ_{o-Ps} (ns)
20	2.21 ± 0.09	0.42 ± 0.10
30	2.17 ± 0.08	0.76 ± 0.10
34	2.41 ± 0.09	0.81 ± 0.11
38	2.51 ± 0.10	0.89 ± 0.11
44	2.55 ± 0.09	0.90 ± 0.11
55	2.93 ± 0.10	0.69 ± 0.15
60	3.04 ± 0.04	0.76 ± 0.06

Table 1 Mean ortho-Positronium (o-Ps) lifetime $\langle\tau_{o-Ps}\rangle$ and distribution σ_{o-Ps} obtained by PALS for DPPC and DPPC:Cer (85:15).

DSC and PALS data comparison (Fig. 2B) confirms that the main changes in slope of the free volume curves as a function of temperature are indeed associated to lipid phase transitions. Moreover, PALS results for DPPC show significant slope changes at both the main gel-fluid transition at 41 – 42 ºC[42], and the tilted ge rippled gel transition, often called "pre-transition",[45] at 34 – 35 ºC, in accordance with DSC results (Fig. 2A).

A combined study of DSC and ^{2}H-NMR was carried out[46] mixtures of sphingomyelin (SM) and Cer, in which either the N-ac chain of sphingomyelin or that of Cer were fully deuterated. ^{2}H-NMR allowed the independent investigation of melting of each lip

Those authors did not study the 15 mol% Cer mixture, but their SM:Cer (80:20 mol ratio) mixture behaved in a very similar way than our DPPC:Cer (85:15 mol ratio). In a previous studyLeung, et al. [46] data for the 10% and 20% mixtures show separately the calorimetric transition curve, the Cer melting (NMR data from deuterated Cer), and the SM melting (NMR data from deuterated SM). As shown in Fig. 2B, there is a lipid population whose behavior departs from that of calorimetry. The use of the NMR technique leads to the conclusion that DSC follows the melting of SM, while Cer melts ~ 10 ºC above. This provides a strong suggestion that, in our case (Fig. 2B) PALS is detecting rather the thermotropic transition of DPPC, while DSC follows the melting of the Cer-enriched domains.

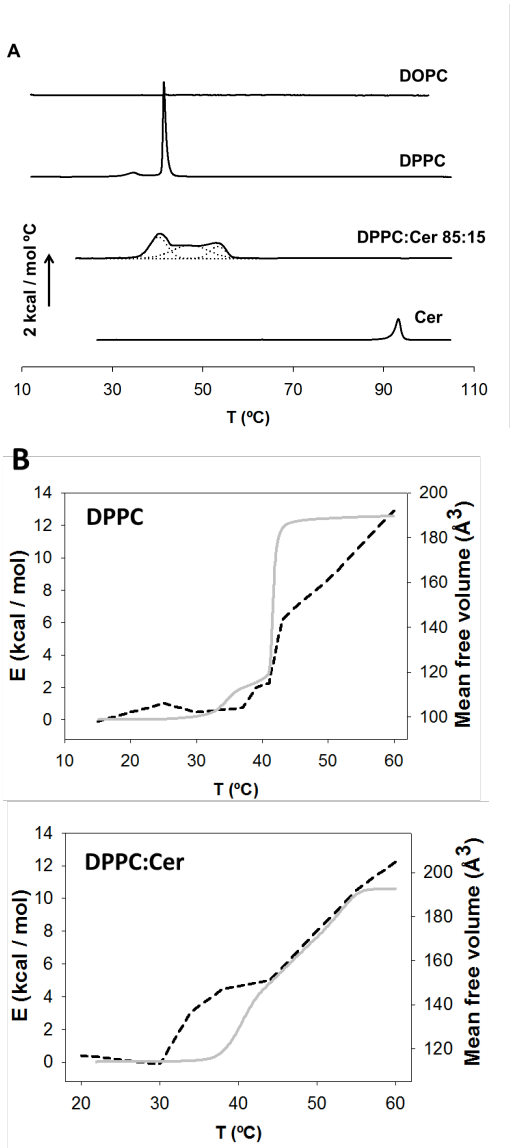

Fig. 2 (A) Differential Scanning Calorimetry (DSC) representative thermograms of DOPC, DPPC, DPPC:Cer 85:15 mol ratio and pure Cer aqueous dispersions. Y axis shows heat capacity (Cp) in kcal/molºC. Dotted lines represent peak fitted endotherms. DPPC Cp values have been divided by a factor of 3 for clarity. (B) Comparison of integrated thermograms (grey solid line) and PALS mean free volumes (black dashed line) for DPPC (above) and DPPC:Cer 85:15 (below).

Atomistic molecular dynamics (MD) simulations of DPPC in solution and a mixture of DPPC and Cer in solution (lipid molecules presented in Fig. 3, left) were carried out at four temperatures: 20 ºC, 30 ºC, 37 ºC and 52 ºC. The final structures corresponding to each simulation are shown in Fig. 4.

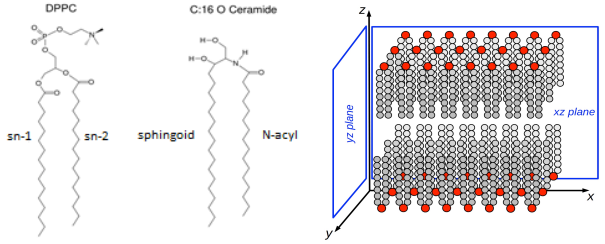

Fig. 3 Left, schematic representation of the two lipid molecules included in the atomistic molecular dynamics simulations. Right, definition of the axis and planes mentioned in the main text.

In accordance with previous studies on the inclusion of Cer in POPC or DMPC bilayers,[47, 48] the MD simulations presented here show that Cer increases the ordering of the lipids. In the electron density profiles evaluated for each simulation (shown in Fig. 5), it can be seen that the DPPC density is lower in the inter-layer area when Cer is present. Moreover, the thickness of the system at the Z axis is significantly larger with Cer. To further quantify this effect, the distance between the centers of mass of the DPPC headgroups located at each leaflet were computed during the last 10 ns of each simulation (shown in Table 2). On one hand, it can be observed for both systems that the larger the temperature, the shorter the distance. On the other hand, the distance length is 5-8 Å larger when Cer is inserted, even though the size of this molecule is smaller. In a previous study.[49] atomic force microscopy-based evidence shows an increase in bilayer thickness of ceramide-enriched domains (in DPPC:pCer supported lipid bilayers) when compared to the surrounding DPPC-enriched continous phase. Note however that these values come from MD simulations only. This confirms what a visual inspection suggests (see Fig. 4): the system is more ordered in the presence of Cer. Interestingly, the density profiles of Cer (orange solid lines in Fig. 5) indicate that these lipids are mainly located in the region where DPPC tails prevail, certainly due to their hydrophobic character. Moreover, the density remains constant in this area, even at the inter-layer domain.

T (ºC)	Distance (Å)	
	DPPC	**DPPC + Cer**
20	40.1 ± 0.2	48.6 ± 0.4
30	39.7 ± 0.3	47.6 ± 0.3
37	37.9 ± 0.5	43.7 ± 0.6
52	36.9 ± 0.4	41.7 ± 0.6

Table 2 Distance (in Å) between the center of masses of DPPC heads located at each leaflet.

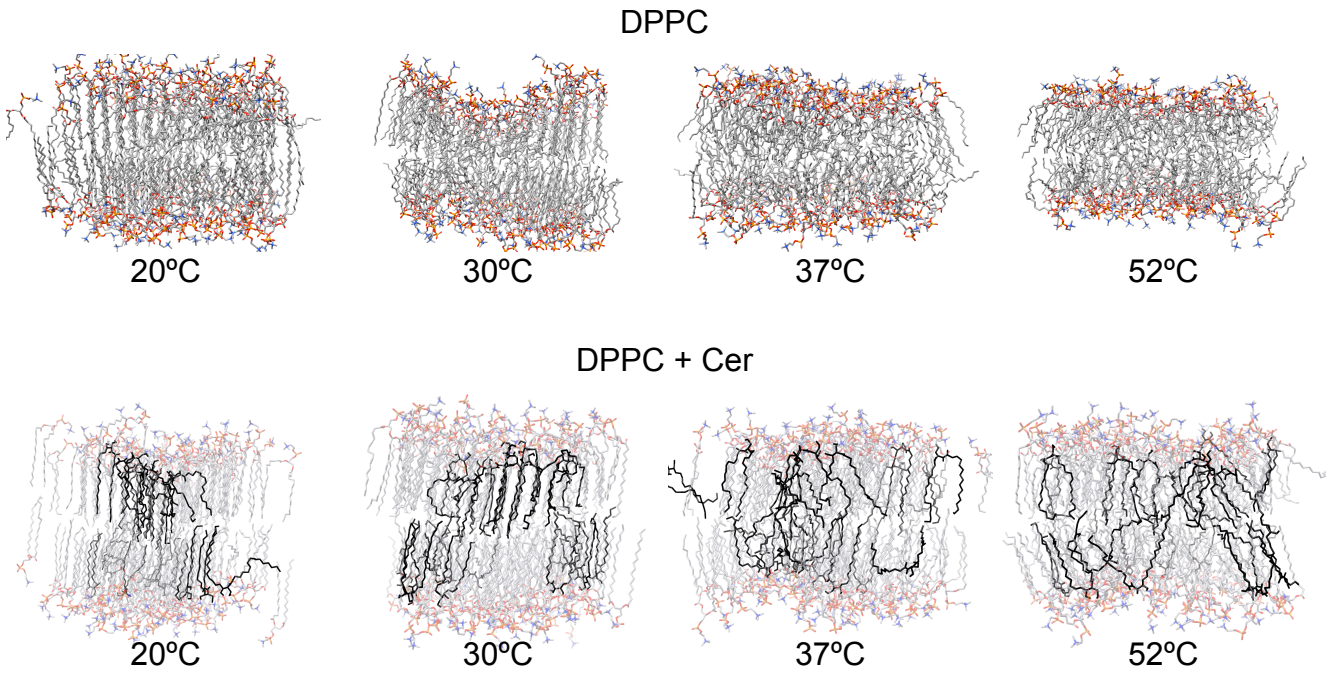

Fig. 4 Final snapshots corresponding to the 100 ns atomistic molecular dynamics simulations carried out for DPPC in water (above) and DPPC + Cer in water (below) at four temperatures: 20 ºC, 30 ºC, 37 ºC and 52 ºC. Cer molecules are shown in black. Note that water molecules are not represented.

In order to further quantify the ordering of lipid tails, the angles formed by each of the carbons located in the acyl chains of DPPC (or Cer) with respect to the bilayer normal plane were calculated. The q_a angle corresponding to C_n carbon is determined by evaluating the angle between the bilayer normal and the vector defined by the C_{n-1} and C_{n+1} atoms. A similar study was previously presented.[50] The calculations were performed for all DPPC and Cer molecules present in the system and averaged over the 10 snapshots taken from the last 10 ns of each simulation. The normalized angle distribution calculated at the XZ and YZ planes are presented in Fig. S1 and Fig. S2 in ESI† for DPPC and Cer, respectively. For DPPC in solution, it can be observed that at the two lowest temperatures (20 ºC and 30 ºC) the angle distribution is narrower than at the two highest temperatures (37 ºC or 52 ºC), indicating that the DPPC chains are more ordered at low temperature. Moreover, the angle peak observed at 20 ºC shows a slight deviation from 0 degrees (especially at the XZ plane), indicating a partial tilted alignment of the lipids. On the other hand, the wider distribution observed at 37 ºC and 52 ºC is a good indication of the more disordered disposition of the lipids, as they are close to or above the phase transition. When Cer lipids are introduced in the system (Fig. S1 in ESI†, right panel), the angle distribution peaks are in general narrower and higher than their counterparts in the DPPC in water system, indicating that the lipid packing has increased. The effect is more pronounced at the two intermediate temperatures, i.e. at 30 ºC and 37 ºC.

The CD bond order parameter is related to the θ_a angle distribution and can be determined in NMR experiments by measuring the deuterium order parameters (S_{CD}). The order parameter tensor, S_{ab}, is defined as:

$$S_{ab} = \frac{1}{2}\left\langle 3\cos\left(\theta_a\right)\cos\left(\theta_b\right) - \delta_{ab}\right\rangle; \quad a,b = x,y,z$$

where θ_a is the angle made by the a^{th} molecular axis with the bilayer normal and δ_{ab} is the Krönecker delta. With united atom force fields, the θ_a angle corresponding to C_n carbon is evaluated as stated above, and S_{CD}^{Sat} is computed as:[48, 51]

$$-S_{CD}^{Sat} = \frac{2}{3}S_{xx} + \frac{1}{3}S_{yy}$$

The CD bond order parameter profiles computed for DPPC and Cer chains are presented in Fig. S3a in ESI†. A value closer to -0.5 indicates high ordering of acyl chains parallel to the bilayer normal. The profiles are in agreement with previous studies[47, 48] and reflect the influence of both the temperature and the inclusion of Cer lipids. For the DPPC system, the S_{CD} value decreases as the temperature increases, indicating that a higher ordering is found at the lowest temperatures. CD bond order for pure DPPC decreases especially beyond the 8th carbon, in accordance with experimental reports for DPPC in fluid phase at 48 ºC[52] and in gel phase[53], the latter depicted in Fig. S3b in ESI† for a direct comparison. Furthermore, the inclusion of Cer increases the ordering at all temperatures and the DPPC chains exhibit nearly constant order until the 11th carbon (and not the 8th). This speaks in favor of Cer as a molecule capable of increasing molecular order along the lipid tails, in agreement with multiple experimental results.[14, 15, 44, 46, 54, 55]

The distributions of free cells along the Z axis evaluated for each simulation are also illustrated in Fig. 5. The data computed at the last 3 snapshots from each simulation are shown in order to give a more complete description of the distribution. As expected, free cells are mainly located in the inner part of the membrane models, while the number of free cells beyond the DPPC headgroups is very small. As the density of DPPC tails increases, the number of free cells also increases, with the largest number at the node plane. However, the distribution at the simulations carried out for the DPPC system show that the increment is not analogous at all temperatures. At 20 ºC and 30 ºC, even if the free volume is significant in the tail region, a neat peak is observed in the membrane node. However, at 37 ºC and 52 ºC a wider peak is observed, indicating that the free volume has increased specially in the region of the lipid tails.

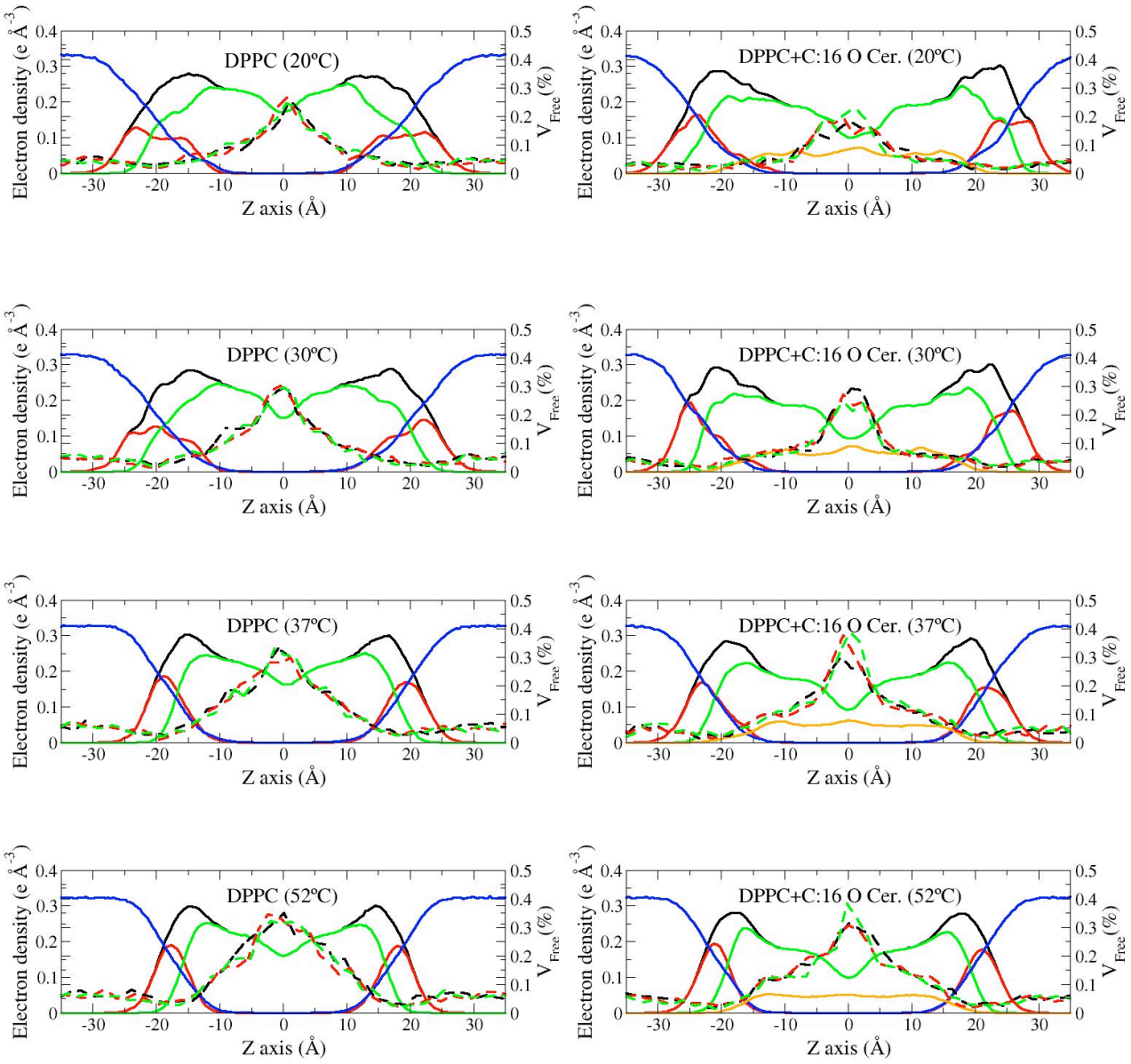

Fig. 5 Electron density profiles (in e/Å^3) along the Z axis calculated for the last 10 ns of the molecular dynamics simulations of DPPC (left) and DPPC + Cer (right) systems at four temperatures (in descending order): 20 ºC, 30 ºC, 37 ºC and 52 ºC. DPPC (solid black), DPPC heads (solid red), DPPC tails (solid green), water (solid blue) and Cer (solid orange). The relative free cell distribution with respect to the Z axis length computed in the last three snapshots extracted from the simulations are shown in dashed lines.

The inclusion of Cer, and the concomitant increment in ordering, has a direct consequence on the free cell distribution. At 20ºC and 30ºC, free cells are in the nodal plane, but the distribution of the peak is wider, due to the increased distance between DPPC lipid tails from each leaflet, which in turn increases bilayer thickness. At higher temperatures, however, the free volume distribution increases in this region, and the peak becomes narrower, resembling the pure DPPC system. In summary, the free cells remain mainly in the nodal plane at all temperatures due to the higher ordering obtained with the inclusion of Cer, but at lower temperatures Cer enhances the space that free cells can occupy in it.

Fig. 6 shows the average void size computed for each system, which can be directly compared with the results obtained from PALS experiments. Due to the size difference between the experimental samples and the MD simulations models, the absolute values of the average void size are significantly smaller than the ones obtained from PALS experiments. However, qualitatively there is a good agreement between the average void size computed from MD simulations and the PALS results. On the one hand, the void average size increases with the temperature. On the other hand, the average void size is larger with Cer, especially at 37 ºC. At 52 ºC the average value is very similar in both systems. As an illustrative example, the three largest voids characterized at the final structure of the simulations carried out for both systems at 37 ºC are illustrated in

Fig. 7. It can be observed that the voids are larger when Cer is present in the system, and that the growing of the voids is mainly due to the larger free volume located at the node plane between the two leaflets.

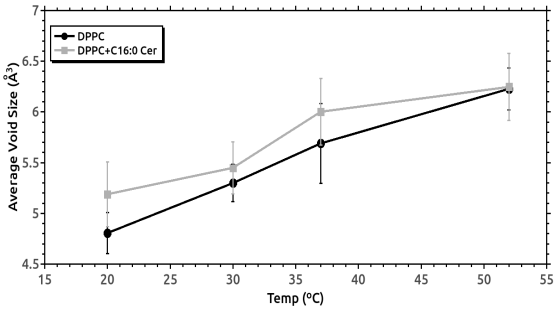

Fig. 6 Computational calculation of average void size (in $Å^3$) at 20 ºC, 30 ºC, 37 ºC and 52 ºC for the DPPC (in black) and DPPC + Cer (in grey) systems.

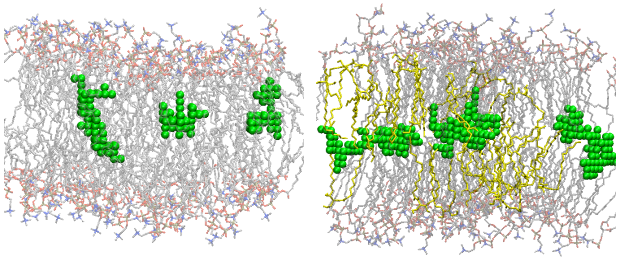

Fig. 7 Representation of the final snapshots from the 100 ns atomistic molecular dynamics simulation for the DPPC (on the left) and DPPC + Cer (on the right) systems at 37 ºC. Cer molecules are shown in yellow. The three largest voids determined in each system are shown in green.

To the best of our knowledge, no previous studies had been performed combining differential scanning calorimetry (DSC) and PALS to provide insights about how lipid membrane free volume is affected by phase transitions in model membranes. In our study, we have used a sealed positron source and a pure aluminum sample holder. This represents a significant advance because the sample is not contaminated with the radioactive sodium and we can extract the source component reliably, at variance with previous studies.[26]

For the studied binary phospholipid:Cer membrane mixtures the appearance of gel Cer-enriched domains has been described from 2% - 3% to 30% Cer in lipid model membranes studied by many different biophysical techniques.[14, 15, 44, 46, 54-58] The well-described broad endotherms that commonly appear in DSC data as a result of the presence of Cer are related to the complex melting process of these gel domains into a fluid state and thermograms can be deconvoluted to multiple endotherms, drifting towards higher temperatures as the Cer ratio is increased. Accordingly, in our data free volume voids also increase in a complex way in these binary mixtures, with slight but noticeable changes in the slope through both transition processes (30 ºC – 55 ºC), suggesting that these complex transitions of the Cer-enriched domains are also related to changes in membrane free volume. DSC data also suggest that at 60 ºC the phase transition processes are completed and no Cer-enriched domains would be expected anymore as lipid bilayers become fluid.

Regarding the atomistic simulation results for pure DPPC, most of the data are well in accordance with previous reports and account for a number of experimental observations. Thus, experiments at 37 ºC for DPPC give some interesting evidence about the rippled gel phase (pre-fluid) due to the reported pretransition of the lipid at 34 – 35ºC. This phase seems to be intermediate between a fluid state and a gel state in terms of CD order (Fig. S3 in ESI†, red solid lines), while chain orientation seems to be closer to the fluid state (Fig. S1 in ESI†, green) This is in agreement with PALS measurements, where the void volume starts to grow after 35 ºC, until a sharp increase is achieved at 41 ºC due to the main gel-fluid transition (Fig. 1). Visual snapshots of pure DPPC bilayers at 37 ºC also support these statements and likely resemble more a fluid state than a gel state (Fig. 4).

The effect of Cer on DPPC lipid bilayers can be summarized as an ordering effect that increases void volumes. Both PALS and MD simulations point to this conclusion. Moreover, MD simulations of the DPPC:Cer 85:15 system show segregation of Cer-enriched domains, particularly below the DPPC main transition (Fig. 4, 20 ºC and 30 ºC). Note that they are not pure Cer domains, but regions in which Cer is particularly abundant; in a previous work [56] a Cer concentration of 30-40 mol% in those rigid domains was estimated. The capacity of Cer to permeabilize lipid bilayers and enhance solute efflux is also a phenomenon whose mechanism has not yet been described in detail. The presence of strictly ceramidic channels has been proposed[59, 60]. However, the free volumes detected by PALS do not support this hypothesis, as they are smaller than expected if a channel was present. Furthermore, MD simulations show voids in the interleaflet region (Fig. 7) and ceramides seem to be present in both the interleaflet and the tails region (Fig. 5), but channels do not appear in the snapshots (Fig. 4 and Fig. 7) and chain orientation for ceramides show that most of them are oriented perpendicularly to the interleaflet plane (0º, Z axis) (Fig. S2 in ESI†). This means that almost no ceramides are detected in the required orientations to form a strictly ceramidic toroid channel, which would require a wider distribution from -90 ºC to 90 ºC.

The fact that MD results show an increase in free volume is also of interest as it suggests that the effect of Cer could not be centered in the Cer-rich domains themselves but in the surrounding continuous phase. The continuous phase surrounding the Cer-enriched domains is estimated to contain a low amount of Cer (~2%)[44, 56], but the effect of Cer in this phase has not been studied in detail. The biophysical effects of the presence of Cer in lipid membranes have been commonly attributed to the segregated domains, with higher nanomechanical resistance and an increased degree of intermolecular packing. The possibility of the free volume being generated at the interphase between the domains and the continuous phase seems plausible as defects in the bilayer could be generated due to inadequate impairing of the different phases, as they have different thicknesses. This would also explain the higher free volume of Cer-containing samples. Note that DPPC:Cer measured by PALS has a higher free volume than pure DPPC even at 60 ºC (Fig. 1), when no domains are present anymore and no endotherms are detected by DSC (Fig. 2), which again shows that Cer is also affecting the free volume of the continuous phase. Nevertheless, more experiments need to be carried out to consolidate these insights. In this regard, future PALS applications to study the effect of ceramide in cholesterol-rich lipid bilayers may be of special interest.

Conclusions

We have described how Cer affects free volume void size and distribution in DPPC membranes. Our data show that the

combination of PALS, DSC and molecular dynamics simulations is a powerful approach for characterizing and understanding free volume in biomembranes. Upon the incorporation of 15 mol% Cer to DPPC, the mean free volume void size increases by up to 40% near the transition temperature. This suggests that the presence of Cer in biomembranes could increase the diffusion within the hydrophobic matrix. We could speculate that poorly understood Cer-promoted processes such as lipid flip-flop motion, the increased membrane permeability, and even the release of cytochrome c to the cytosol from mitochondria in apoptosis, are assisted by these changes in the free volume of the membranes. The reference to apoptosis is relevant, as disorders linked to cell death are related to diseases such as cancer for which ceramide is considered a potential therapeutic target.[61, 62] A better understanding of the biophysical effects of ceramide and the mechanisms involved in cell death processes could contribute to the improvement of ceramide-related anti-cancer therapies, and the implications of the increase in free volume voids due to ceramide require further research.

Acknowledgments

EA and AGA gratefully acknowledge the Basque Department of Education, Universities and Research funding (IT-443-10). JIM recognizes the Basque Government (GIC IT588-13) and the Spanish Ministerio de Economía y Competitividad (MINECO) (CTQ2012-38496-C05-01 and CTQ2012-38496-C05-04). This work was also supported in part by grants from the Spanish Government (MINECO BFU 2012-36241 to F.M.G. and BFU 2011-28566 to A.A.) and the Basque Government (IT849-13 to F.M.G: and IT838-13 to A.A.). The SGI/IZO-SGIker UPV/EHU is also acknowledged for computational resources.

Notes and references

[a] Department of Electricity and Electronics, University of the Basque Country (UPV/EHU), Leioa, Basque Country, Spain.

[b] Unidad de Biofísica (CSIC, UPV/EHU), 48940 Leioa, Spain.

[c] Departamento de Bioquímica, University of the Basque Country (UPV/EHU), 48080 Bilbao, Spain.

[d] Kimika Fakultatea, Euskal Herriko Unibertsitatea (UPV/EHU) and Donostia International Physics Center (DIPC), Donostia, Basque Country, Spain.

[e] Department of Applied Physics II, University of the Basque Country (UPV/EHU), Leioa, Basque Country, Spain.

[CO] These authors contributed equally to these work.

† Electronic Supplementary Information (ESI) available: normalized angle distributions computed for the DPPC and for the Cer acyl chain C atoms during the atomistic MD, S_{CD} order parameter profiles for sn-1 and sn-2 acyl chain C atoms of DPPC and Cer, and the comparison between CD order parameters measured for sn-2 acyl chains of pure DPPC experimentally by ^{2}H-NMR and our MD profile at 20 ºC. See DOI: 10.1039/b000000x/

1. A. Gómez-Muñoz, *Biochimica et biophysica acta*, 1998, 1391, 92-109.
2. Y. A. Hannun, C. R. Loomis, A. H. Merrill, Jr. and R. M. Bell, *The Journal of biological chemistry*, 1986, 261, 12604-12609.
3. A. Merrill, A. Sereni, V. Stevens, Y. Hannun, R. Bell and J. Kinkade, *Journal of Biological Chemistry*, 1986, 261, 12610-12615.
4. R. N. Kolesnick, *The Journal of biological chemistry*, 1987, 262, 16759-16762.
5. S. N. Pinto, L. C. Silva, A. H. Futerman and M. Prieto, *Biochimica et biophysica acta*, 2011, 1808, 2753-2760.
6. L. M. Obeid, C. M. Linardic, L. A. Karolak and Y. A. Hannun, *Science*, 1993, 259, 1769-1771.
7. A. Cremesti, F. Paris, H. Grassme, N. Holler, J. Tschopp, Z. Fuks, E. Gulbins and R. Kolesnick, *The Journal of biological chemistry*, 2001, 276, 23954-23961.
8. R. Kolesnick, *The Journal of clinical investigation*, 2002, 110, 3-8.
9. F. M. Goñi and A. Alonso, *Biochimica et Biophysica Acta (BBA)-Biomembranes*, 2009, 1788, 169-177.
10. L. R. Montes, M. B. Ruiz-Arguello, F. M. Goñi and A. Alonso, *The Journal of biological chemistry*, 2002, 277, 11788-11794.
11. M. B. Ruiz-Arguello, G. Basañez, F. M. Goñi and A. Alonso, *The Journal of biological chemistry*, 1996, 271, 26616-26621.
12. F. X. Contreras, A. V. Villar, A. Alonso, R. N. Kolesnick and F. M. Goñi, *The Journal of biological chemistry*, 2003, 278, 37169-37174.
13. S. Hartel, M. L. Fanani and B. Maggio, *Biophysical journal*, 2005, 88, 287-304.
14. J. M. Holopainen, M. Subramanian and P. K. Kinnunen, *Biochemistry*, 1998, 37, 17562-17570.
15. L. C. Silva, R. F. de Almeida, B. M. Castro, A. Fedorov and M. Prieto, *Biophysical journal*, 2007, 92, 502-516.
16. J. Sot, F. J. Aranda, M. Collado, F. M. Goñi and A. Alonso, *Biophysical journal*, 2005, 88, 3368-3380.
17. J. Sot, L. A. Bagatolli, F. M. Goni and A. Alonso, *Biophysical journal*, 2006, 90, 903-914.
18. L. R. Montes, D. J. Lopez, J. Sot, L. A. Bagatolli, M. J. Stonehouse, M. L. Vasil, B. X. Wu, Y. A. Hannun, F. M. Goñi and A. Alonso, *Biochemistry*, 2008, 47, 11222-11230.
19. H. Lee, J. A. Rotolo, J. Mesicek, T. Penate-Medina, A. Rimner, W.-C. Liao, X. Yin, G. Ragupathi, D. Ehleiter and E. Gulbins, *PLoS One*, 2011, 6, e19783.
20. M. Kupiainen, E. Falck, S. Ollila, P. Niemelä, A. Gurtovenko, M. Hyvönen, M. Patra, M. Karttunen and I. Vattulainen, *Journal of Computational and Theoretical Nanoscience*, 2005, 2, 401-413.
21. M. Javanainen, L. Monticelli, J. B. de la Serna and I. Vattulainen, *Langmuir*, 2010, 26, 15436-15444.
22. S. J. Marrink and H. J. Berendsen, *The Journal of Physical Chemistry*, 1996, 100, 16729-16738.
23. P. Almeida and W. Vaz, *Handbook of biological physics*, 1995, 1, 305-357.
24. D. Bemporad, C. Luttmann and J. Essex, *Biophysical journal*, 2004, 87, 1-13.
25. Y. Jean and A. Hancock, *The Journal of Chemical Physics*, 1982, 77, 5836-5839.
26. P. Sane, E. Salonen, E. Falck, J. Repakova, F. Tuomisto, J. M. Holopainen and I. Vattulainen, *The journal of physical chemistry. B*, 2009, 113, 1810-1812.
27. E. Axpe, T. Lopez-Euba, A. Castellanos-Rubio, D. Merida, J. A. Garcia, L. Plaza-Izurieta, N. Fernandez-Jimenez, F. Plazaola and J. R. Bilbao, *PLoS One*, 2014, 9, e83838.
28. J. Kansy, *Nuclear Instruments and Methods in Physics Research Section A: Accelerators, Spectrometers, Detectors and Associated Equipment*, 1996, 374, 235-244.
29. M. Eldrup, D. Lightbody and J. N. Sherwood, *Chem Phys*, 1981, 63, 51-58.

30. S. J. Tao, *J Chem Phys*, 1972, 56, 5499-&.
31. H. Nakanishi, S. Wang, Y. Jean and S. Sharma, *World Science, Singapore*, 1988, 292.
32. Peter Tieleman's Biocomputing Group, http://www.ucalgary.ca/tieleman/?page=Structures_and_Topologies (accessed June 2014).
33. Roland Faller Research Group, http://www.chms.ucdavis.edu/research/web/faller/ (accessed June 2014).
34. D. Van Der Spoel, E. Lindahl, B. Hess, G. Groenhof, A. E. Mark and H. J. Berendsen, *Journal of computational chemistry*, 2005, 26, 1701-1718.
35. B. Hess, C. Kutzner, D. Van Der Spoel and E. Lindahl, *Journal of chemical theory and computation*, 2008, 4, 435-447.
36. O. Berger, O. Edholm and F. Jähnig, *Biophysical journal*, 1997, 72, 2002-2013.
37. W. G. Hoover, *Physical review. A*, 1985, 31, 1695-1697.
38. S. Nosé and M. Klein, *Molecular Physics*, 1983, 50, 1055-1076.
39. U. Essmann, L. Perera, M. L. Berkowitz, T. Darden, H. Lee and L. G. Pedersen, *J Chem Phys*, 1995, 103, 8577-8593.
40. B. Hess, H. Bekker, H. J. Berendsen and J. G. Fraaije, *Journal of computational chemistry*, 1997, 18, 1463-1472.
41. J. Čížek, I. Procházka, O. Morozova, C. Borchers and A. Pundt, *Journal of Applied Physics*, 2010, 107, 043509.
42. D. Chapman and D. T. Collin, *Nature*, 1965, 206, 189.
43. N. Jiménez-Rojo, A. B. García-Arribas, J. Sot, A. Alonso and F. M. Goñi, *Biochimica et Biophysica Acta (BBA)-Biomembranes*, 2014, 1838, 456-464.
44. D. C. Carrer and B. Maggio, *J Lipid Res*, 1999, 40, 1978-1989.
45. M. J. Janiak, D. M. Small and G. G. Shipley, *Biochemistry*, 1976, 15, 4575-4580.
46. S. S. Leung, J. V. Busto, A. Keyvanloo, F. M. Goni and J. Thewalt, *Biophysical journal*, 2012, 103, 2465-2474.
47. B. Dutagaci, J. Becker-Baldus, J. D. Faraldo-Gomez and C. Glaubitz, *Biochimica et biophysica acta*, 2014, 1838, 2511-2519.
48. S. A. Pandit, S.-W. Chiu, E. Jakobsson, A. Grama and H. Scott, *Biophysical journal*, 2007, 92, 920-927.
49. A. B. Garcia-Arribas, J. V. Busto, A. Alonso and F. M. Goni, *Langmuir*, 2015.
50. S. Leekumjorn and A. K. Sum, *Biochimica et Biophysica Acta (BBA)-Biomembranes*, 2007, 1768, 354-365.
51. J.-P. Douliez, A. Leonard and E. J. Dufourc, *Biophysical journal*, 1995, 68, 1727-1739.
52. T. Mehnert, K. Jacob, R. Bittman and K. Beyer, *Biophysical journal*, 2006, 90, 939-946.
53. J. Seelig and A. Seelig, *Biochem Biophys Res Commun*, 1974, 57, 406-411.
54. Y.-W. Hsueh, R. Giles, N. Kitson and J. Thewalt, *Biophysical journal*, 2002, 82, 3089-3095.
55. H.-W. Huang, E. M. Goldberg and R. Zidovetzki, *Biochemical and biophysical research communications*, 1996, 220, 834-838.
56. J. V. Busto, M. L. Fanani, L. De Tullio, J. Sot, B. Maggio, F. M. Goñi and A. Alonso, *Biophysical journal*, 2009, 97, 2717-2726.
57. M. Fidorra, L. Duelund, C. Leidy, A. C. Simonsen and L. A. Bagatolli, *Biophysical journal*, 2006, 90, 4437-4451.
58. M. P. Veiga, J. L. R. Arrondo, F. M. Goñi and A. Alonso, *Biophysical journal*, 1999, 76, 342-350.
59. L. J. Siskind, R. N. Kolesnick and M. Colombini, *The Journal of biological chemistry*, 2002, 277, 26796-26803.
60. L. J. Siskind, R. N. Kolesnick and M. Colombini, *Mitochondrion*, 2006, 6, 118-125.
61. B. M. Barth, M. C. Cabot and M. Kester, *Anti-cancer agents in medicinal chemistry*, 2011, 11, 911-919.
62. S. A. Morad and M. C. Cabot, *Nature Reviews Cancer*, 2012, 13, 51-65.

Graphical Abstract